Self-dual pattern spectra for characterising the dermal-epidermal junction in 3D reflectance confocal microscopy imaging

Julie Robic, Benjamin Perret, Alex Nkengne, Michel Couprie, Hugues Talbot

Self-dual pattern spectra for characterising the dermal-epidermal junction in 3D reflectance confocal microscopy imaging.

Julie Robic[1,2], Benjamin Perret[2], Alex Nkengne[1], Michel Couprie[2], and Hugues Talbot[2,3]

[1] Laboratoires Clarins, Pontoise, France.
[2] Université Paris-Est, Laboratoire d'Informatique Gaspard-Monge UMR 8049, UPEMLV, ESIEE Paris, ENPC, CNRS, France.
[3] CentraleSupélec, Centre de Vision Numérique, INRIA, France.

Abstract. The Dermal-Epidermal Junction (DEJ) is a 2D surface separating the epidermis from the dermis which undergoes multiple changes under pathological or ageing conditions. Recent advances in reflectance confocal microscopy now enables the extraction of the DEJ from in-vivo imaging. This articles proposes a method to automatically analyse DEJ surfaces using self-dual morphological filters. We use self-dual pattern spectra with non-increasing attributes and we propose a novel measure in order to characterize the evolution of the surface under the filtering process. The proposed method is assessed on a specifically constituted dataset and we show that the proposed surface feature significantly correlates with both chronological ageing and photo-ageing.

Keywords: Pattern spectrum · Tree-of-Shapes · 2D surface · skin.

1 Introduction

We address the problem of automatically characterizing a specific structure of the skin, the Dermal-Epidermal Junction (DEJ), in in-vivo Reflectance Confocal Microscopy (RCM) 3D images. The DEJ is a complex, surface-like, 2D boundary, separating the epidermis from the dermis, which undergoes multiple changes under pathological or ageing conditions (see Figure 1). In particular, alterations of the DEJ modify the regularity and the depth of its peaks and valleys, called dermal papillae [6,12]. Automated analysis of RCM images of the skin is a challenging task due to the very low signal to noise ratio and the important blur present in the acquisitions.

In previous work [15,13], we have presented a method to obtain reliable segmentation of the DEJ in RCM images using 3D conditional random fields embedding biological prior (see Figure 1). Moreover, the proposed method guarantees that the segmented region of the 3D RCM image is indeed a 2D topological surface defined on a regular grid, *i.e.*, an elevation/topographic map.

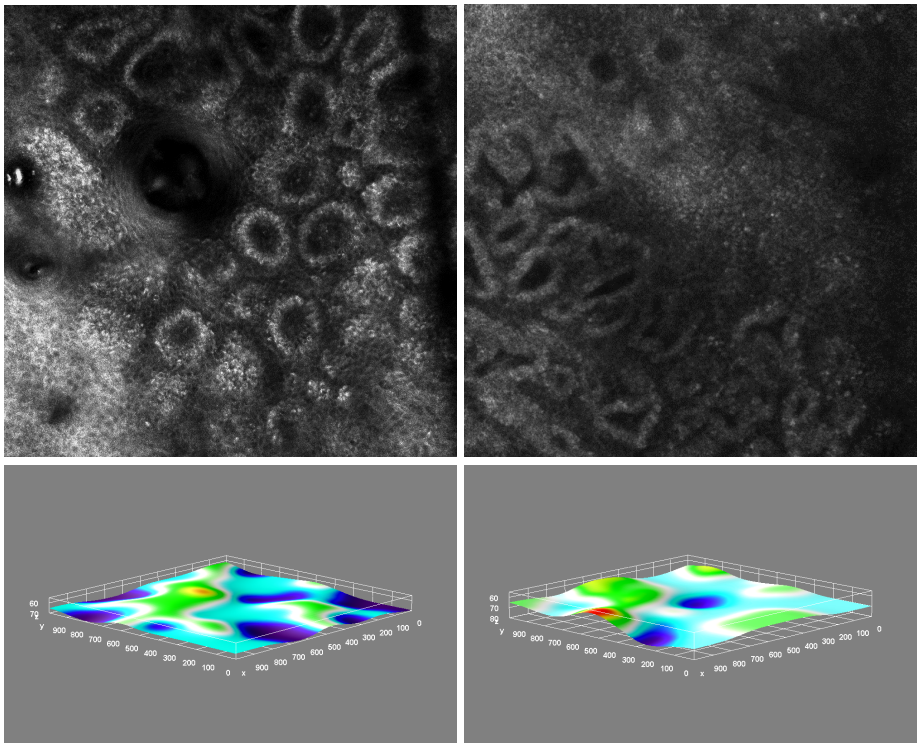

(a) Young subject (b) Aged subject

Fig. 1: DEJ ageing. First row: en-face sections of 2 RCM stacks coming respectively from a young (a) and an older (b) subject. The DEJ corresponds to the brightest rings. Second row: automatically segmented DEJ surfaces from a young (a) and an older (b) subject using the method desribed in [15].

Besides this, granulometries and pattern spectra [10] are standard morphological tools for characterizing the content of an image. Their principle is to iteratively apply a sequence of increasing filters and to measure the evolution of the filtered image. Their extension to attribute connected filters [17], is widely used to obtain efficient and powerful multi-scale features using tree based representations of images that enable a region-based analysis, rather than a pixel-based one. In particular, attribute profiles [4] are now a standard approach to compute pixel-wise features for the semantic segmentation of high-resolution remote sensing images.

Moreover, their self-dual extension [3,9], using the Tree-of-Shapes image representation [11] (also called tree of level lines or inclusion tree), have been shown to increase the performances of classifiers. In such a representation, each level line (or iso-contour) of the surface is the boundary of a region of interest. Then, the inclusion relation between the various level lines of the surface forms a tree

structure: this representation is called the Tree-of-Shapes. This representation benefits from several useful properties: it is invariant to scaling, rotations, translations, and monotone contrast modifications. This last invariance also implies that the Tree-of-Shapes is a self-dual representation, *i.e.*, that the inversion of the topographic surface (where peaks become valleys and conversely) does not modify the representation.

The objective of this article is to provide a method for automatically characterizing a DEJ surface with the objective to quantify the ageing process. As our DEJ surfaces are indeed elevation maps, it is thus possible to analyse them using morphological representations such as the Tree-of-Shapes. An example of a DEJ topographic surface, its level lines, and the corresponding Tree-of-Shapes are presented in Figure 2. From the DEJ surface, we next compute self-dual pattern spectra, with the following desirable properties:

1. the ability to select the attribute guiding the filtering according to the dermatologists' analysis;
2. providing an analytic formulation of the algorithm generalizing the subtractive filtering rule [17] to non increasing attribute filters on the Tree-of-Shapes proposed in [2];
3. the definition a novel measure in order to characterize the filtered surfaces.

The proposed method is assessed on a specifically constituted dataset involving 15 persons divided in two age groups. Our results show that the proposed characterization of the DEJ surface is significantly correlated with both chronological ageing and photo-ageing.

This article is organized as follows. Section 2 recalls the definition of the Tree-of-Shapes. Section 3 defines subtractive self-dual attribute filters and related pattern spectra. The parameters of the method and their biological significance are discussed in Section 4. Finally, Section 5 presents the assessment of the proposed method and discusses the results.

2 Tree of shapes

In this section, we review the definition of the Tree-of-Shapes. We mainly follow the formalism proposed in [1].

A DEJ surface is modelled by a *topographic map*, *i.e.*, a function f from a non empty finite rectangular subset E of $\mathbb{Z}^2$ to $\mathbb{R}$. An element of E is called *a point*. The value of f at a point x of E is called the *elevation or level of f at x*.

Let $X \subseteq E$, we denote by $CC_x(X)$ the connected component of X that contains the pixel x using the classical 4-adjacency on the discrete grid. We denote by $CC(X)$ the set of connected components of X: $CC(X) = \{CC_x(X),\ x \in X\}$. Moreover, we assume that E is connected: *i.e.*, $CC(E) = \{E\}$.

Given a topographic map f, the *upper-level set* (respectively *lower-level set*) of f at level k in $\mathbb{R}$, denoted by $[f > k]$ (respectively $[f < k]$), is the set of pixels

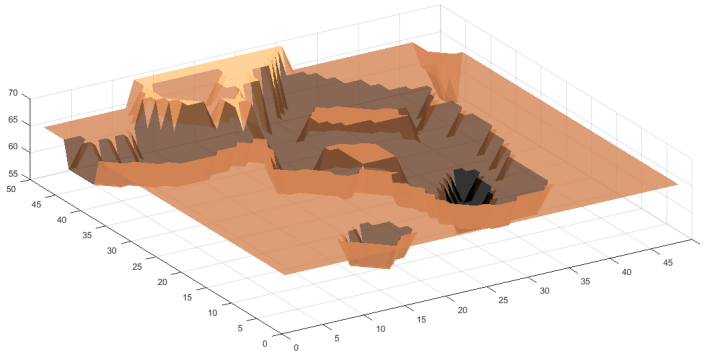

(a) Segmented DEJ as a 2D surface

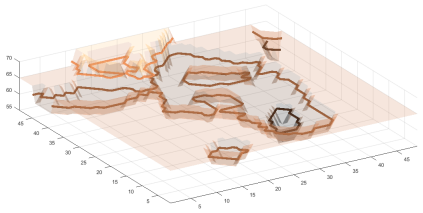

(b) Level lines of the 2D surface in (a)

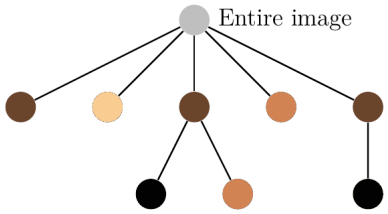

(c) Tree-of-Shapes shown in (b)

Fig. 2: Example of DEJ segmentation as a topographic surface. In (a), the DEJ segmentation is presented in 3D. Each level line is the contour of a level set of the surface (b). In (c), the Tree-of-Shapes induced by the inclusion relationship between the level lines.

where the elevation of f is larger than k (respectively lower than k):

$$[f > k] = \{x \in E \mid f(x) > k\}\,, \text{and} \tag{1}$$
$$[f < k] = \{x \in E \mid f(x) < k\}\,. \tag{2}$$

While the set of connected components of the upper-level (respectively lower-level) sets of f enables to define the classical Max-Tree [16] (respectively Min-Tree) which is oriented toward the maxima (respectively the minima) of f, considering the union of both enables to define a new structure, the Tree-of-Shapes, that represents equally the minima and the maxima of f.

Let X be a connected subset of E, the *saturation of* X denoted $\text{sat}(X)$, is the set defined as the union of X and its *holes*. Formally, one can define $\text{sat}(X)$ equals to $CC_{p_\infty}(X^c)^c$, where p_∞ is an arbitrary point designing the exterior of E (usually taken on the border of E) and where, given a subset Y of E, Y^c is the complement of Y in E, *i.e.*, $Y^c = \{x \in E \mid x \notin Y\}$. The saturation of a connected component of a lower/upper level set of a topographic map of f is called a *shape of* f and the set of shapes of f is denoted by $\mathcal{S}(f)$. The level lines of

the topographic map f are the contours of the shapes $\mathcal{S}(f)$. Note that, to ensure that each level line of f is an isolated closed curve, we used the intermediate continuous multivalued function representation proposed in [5].

Let f be a topographic map. The inclusion relation on the set of shapes $\mathcal{S}(f)$ induces a tree structure called the *Tree-of-Shapes* (see Figure 3). Given two distinct shapes s_1 and s_2 in $\mathcal{S}(f)$, we say that s_2 is *a child of* s_1, and that s_1 is *the parent of* s_2, if s_2 is included in s_1 and if it is maximal for this condition: *i.e.*, for any shape s_3 in $\mathcal{S}(f)$ such that $s_2 \subseteq s_3 \subset s_1$ then $s_2 = s_3$. For any shape s in $\mathcal{S}(f)$ different from E, the unique parent of s is denoted $\mathrm{Par}(s)$. By abuse of notation, we set $\mathrm{Par}(E)$ equals to E. Given a shape s in $\mathcal{S}(f)$, the set of children of s is denoted $\mathrm{Ch}(s)$.

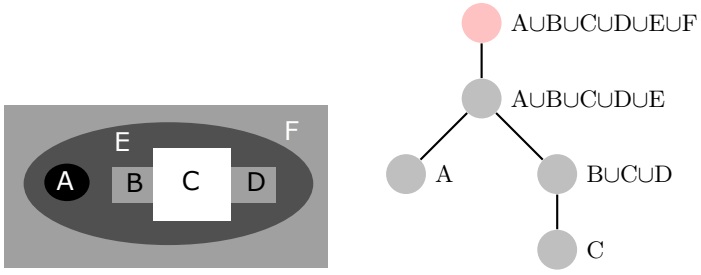

Fig. 3: Tree-of-Shapes of a topographic map. The root of the tree is at the top represented by a red circle.

Let f be a topographic map. Given a shape s in $\mathcal{S}(f)$, the *proper points of* s, denoted by $\mathrm{Pro}(s)$ is the non empty subset of points of s that do not belong to any child of s: *i.e.*, $\mathrm{Pro}(s) = s \setminus \bigcup \mathrm{Ch}(s)$. Given a shape s in $\mathcal{S}(f)$, the elevation of f is constant on $\mathrm{Pro}(s)$: it is called *the level of* s and it is denoted by $\mathrm{Lvl}(s)$.

3 Attribute profiles and pattern spectra

An attribute profile of a topographic map is obtained by the application of a sequence of *increasing* morphological filters [10,17]: the sequence of results then provides a multi-scale characterization of the map highlighting the features selected by the filters. While attribute profiles can be used directly as features for point-wise segmentation [4], global features can be defined by considering the evolution of some measure, such as the volume or the area, on the filtered maps: this is then called a pattern spectrum of the map [10,17]. In the context of this article, we define attribute profiles and pattern spectra in the particular case of self-dual attribute connected filters; more general definitions can be found in the previously cited articles.

Let f be a topographic map. An attribute on $\mathcal{S}(f)$ is a function A from $\mathcal{S}(f)$ to $\mathbb{R}^+$. In general A is not an increasing function and some care must be taken

in order to define the result of a filtering of f by A: this issue has been studied in the context of the Max-Tree in [16] and, for the construction of attribute profiles, the subtractive rule is usually chosen [17]. The authors of [2] proposed an algorithm to extend the subtractive filtering rule to the case of of the Tree of Shapes, for which we give an analytic formulation in the followings paragraph.

In the original definition of the subtractive rule in [17], the level of a point in the filtered map is obtained by counting the number of non deleted components under it in the original map. To generalize this idea to a Tree-of-Shapes based filter, one must take into account that node levels are not necessarily increasing in such trees: counting nodes is thus not a useful method to retrieve meaningful levels. Instead, for any shape s, we consider the *contrast of* s, denoted by $\mathrm{cont}(s)$, and defined as the difference between the level of the shape s and the level of its parent, which can be positive or negative: *i.e.*, $\mathrm{cont}(s) = \mathrm{Lvl}(s) - \mathrm{Lvl}(\mathrm{Par}(s))$. Then, the new level of a filtered shape s is equal to its original level minus the contrast of every deleted ancestors of this shape. Formally, the subtractive self-dual attribute filter $\sigma_A(f,k)$ of f by A at threshold $k \in \mathbb{R}^+$ is defined by:

$$\forall x \in E, \sigma_A(f,k)(x) = \mathrm{Lvl}(\min\{s \in \mathcal{S}(s) \mid x \in s, \text{and } A(s) \geq k\}) - \sum_{\substack{q \in \mathcal{S}(s) \\ s \subset q, A(q) < k}} \mathrm{cont}(q), \quad (3)$$

i.e., the level of the smallest non deleted shape containing x minus the contrast of every deleted shapes containing x. Applications of the subtractive self-dual attribute filter are illustrated in Figure 4.

The *self-dual attribute profiles of the topographic map* f for the subtractive self-dual attribute filter σ_A by the attribute A is then defined as the partial function application $\sigma_A(f,\cdot)$: *i.e.*, the function that associates the result of the subtractive self-dual attribute filter $\sigma_A(f,k)$ to a threshold value $k \in \mathbb{R}^+$.

Finally, given a measure ξ that associates a single real value to any topographic map and a self-dual attribute profiles $\sigma_A(f,\cdot)$, the pattern spectrum $\rho_A^\xi(f)$ of the topographic map f for A is defined as the function:

$$\rho_A^\xi(f) = \frac{d(\xi \circ \sigma_A(f,\cdot))}{dk}, \quad (4)$$

i.e., the derivative of the function that associates the measure of $\sigma_A(f,\cdot)$ for ξ to a threshold value $k \in \mathbb{R}$.

4 Choice of the attribute and of the measure

Two parameters need to be determined to define a pattern spectrum of a DEJ: the attribute guiding the filtering process and the measure characterizing the result of the filters.

Concerning the choice of the filtering criterion, visual analysis made by dermatologist [7,8] have shown that the regularity of the dermal papillae, *i.e.*, the

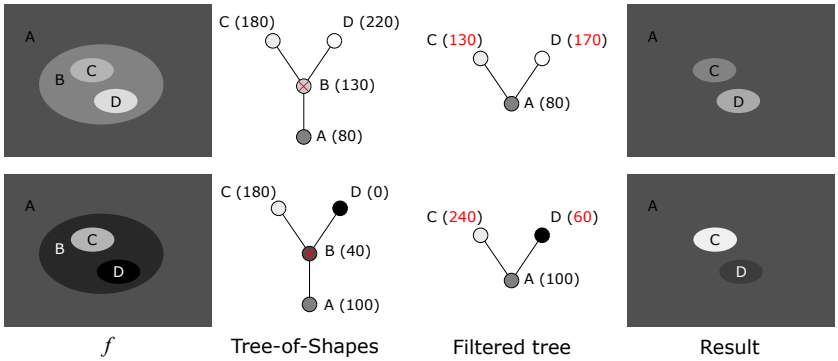

Fig. 4: Self-dual attribute filter with the subtractive rule. Each row shows the filtering of a map f composed of 4 regions (first column). The second column shows the Tree-of-Shapes of f with the node levels in parenthesis. The third column shows the filtered tree, and finally, the last column shows the filtered map. In each case, the shape corresponding to the region B is removed by the filter. In the first case, the Tree-of-Shapes is equal to the Max-Tree of f and the result is identical to the one obtained with the classical definition of the subtractive rule [17].

peaks and the valleys of the DEJ, decreases with age. Therefore, we propose to use the compactness attribute during the filtering process. Formally, the compactness $\mathrm{comp}(s)$ of a shape $s \subseteq E$ is defined as:

$$\mathrm{comp}(s) = \frac{4\pi\,\mathrm{area}(s)}{\mathrm{perimeter}(s)^2}, \tag{5}$$

where $\mathrm{area}(s)$ is the number of points in s and $\mathrm{perimeter}(s)$ is the length of the perimeter of s. The compactness is a scale and rotation invariant measure that is maximal for a circle with a value of 1 and that tends toward 0 as the shape regularity decreases. An illustration of the DEJ surface evolution undergoing a filtering process with a compactness criterion is presented in Figure 5.

Then, we need to determine the measure to be extracted at each filtering step. As the DEJ is a 2D surface, separating the epidermis from the dermis, we aim to compute an attribute in connection with the DEJ anatomy. Among all possible criteria, the surface area is a good candidate to obtain global information on the complexity of the surface as it is directly linked to the number, depth and shape of the peaks and the valleys in the DEJ.

We define the *surface area of a shape* s, denoted by $\mathrm{sarea}(s)$, recursively as:

$$\mathrm{sarea}(s) = \mathrm{area}(s) + \mathrm{perimeter}(s) \times \mathrm{cont}(s) + \sum_{c \in \mathrm{Ch}(s)} \left(\mathrm{sarea}(c) - \mathrm{area}(c)\right), \tag{6}$$

where the second part of the equation adds up the surface area of the children $\mathrm{Ch}(s)$ of s minus their area, which is already counted in the area of s. An example

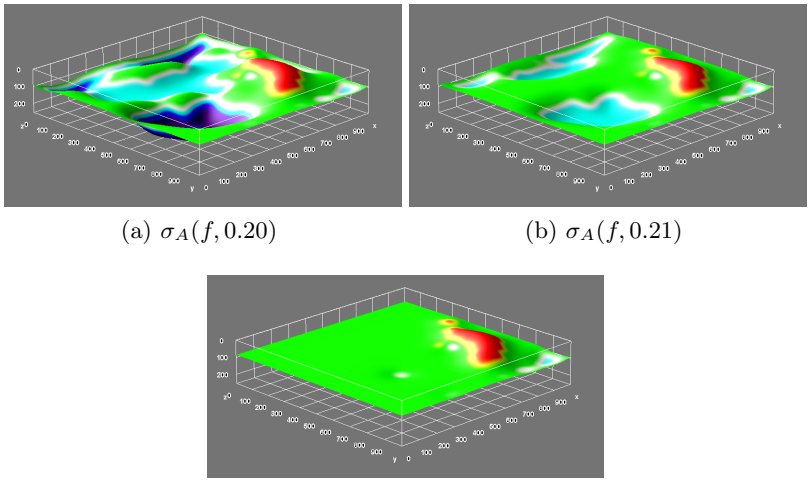

(a) $\sigma_A(f, 0.20)$ (b) $\sigma_A(f, 0.21)$

(c) $\sigma_A(f, 0.22)$

Fig. 5: Filtering of a DEJ surface f with a compactness criterion. In each case, the threshold value is indicated in the figure caption.

of the surface area attribute is presented in Figure 6. The surface area attribute differs from the area attribute in the way that it takes into account the level of a node which, in our case, encodes the location in depth of the corresponding region in the 3D segmentation. The surface area attribute can be computed efficiently in linear time using Algorithm 1. The surface area attribute is calculated from the leaves up to the root of the tree. First, the product of the perimeter and contrast is calculated from the leaves to the root of the tree. Second, the area of each node (with its holes filled) is added to their corresponding surface area attribute. One can note that all the parameters of the algorithm (*e.g.*, the perimeter length of the shapes) can also be computed efficiently [18].

Algorithm 1: Surface area attribute.

Input : A Tree-of-Shapes *tree*, and the three functions area, perimeter and cont on the nodes of the tree.
Output: The surface area attribute.

```
for all nodes i of tree do sarea(i) := 0 ;
for all nodes i of the tree from the leaves to the root (excluded) do
    sarea(i)+ = cont(i) × perimeter(i) ;
    sarea(Par(i))+ = sarea(i) ;
end
for all nodes i of tree do sarea(i)+ = area(i) ;
return S;
```

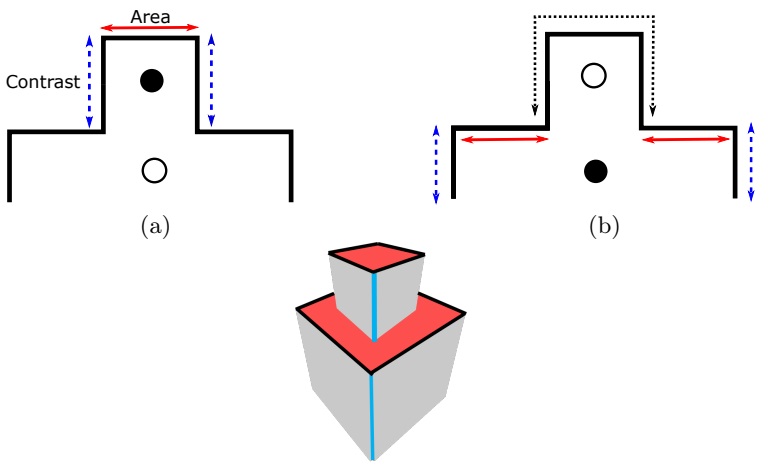

Fig. 6: Computation of the surface area. The surface area is the sum of the area (red arrows) and the contrast $\times$ perimeter (blue arrows). In (a) the attribute is calculated on a leaf of the tree. In (b) it is calculated on its parent. A 3D representation of the surface area attribute is shown in (c). The red areas correspond to the area of the corresponding nodes. The contrast (blue lines) $\times$ perimeter (black lines) is calculated to obtain the grey areas which are added to the red areas to finally obtain the surface area attribute.

One can note that the surface area of the root (*i.e.*, the surface area of the whole topographic map) is equal to the discrete variation of the map plus the area of its domain. Moreover, as the pattern spectrum $\rho^{\text{sarea}}_{\text{comp}}$ measures the evolution of the surface area, the area terms cancel each other out, and the pattern spectrum then measures the evolution of the total variation of the surface.

The whole pattern spectrum of a topographic map f can be computed exactly and efficiently: for each shape by increasing value of compactness λ, subtract the product of the perimeter by the contrast of the shape to the surface area of the root node in order to obtain $\xi \circ \sigma_A(f, \lambda)$.

5 Experiments

In the following experiments, we assess the variability of the proposed DEJ characterisation between two groups of patients with different ages. Fifteen healthy volunteers with fair skin were enrolled in this study. Volunteers were assigned to two groups: a 7-person group aged from 18 to 25 and another 8-person group aged from 55 to 65. Our investigations were carried out on the cheek to assess chronological ageing, the dorsal forearm and the volar arm to assess photo-

ageing. No cosmetic products or skin treatment were allowed on the day of the acquisitions. Appropriate consent was obtained from all subjects before imaging. Distributions are compared using a two-sample Kolmogorov-Smirnov test and and the statistics significance is defined as follow:

1. *: $0.01 < \text{P-values} \leq 0.05$;
2. **: $0.001 < \text{P-values} \leq 0.01$;
3. ***: $\text{P-values} \leq 0.001$.

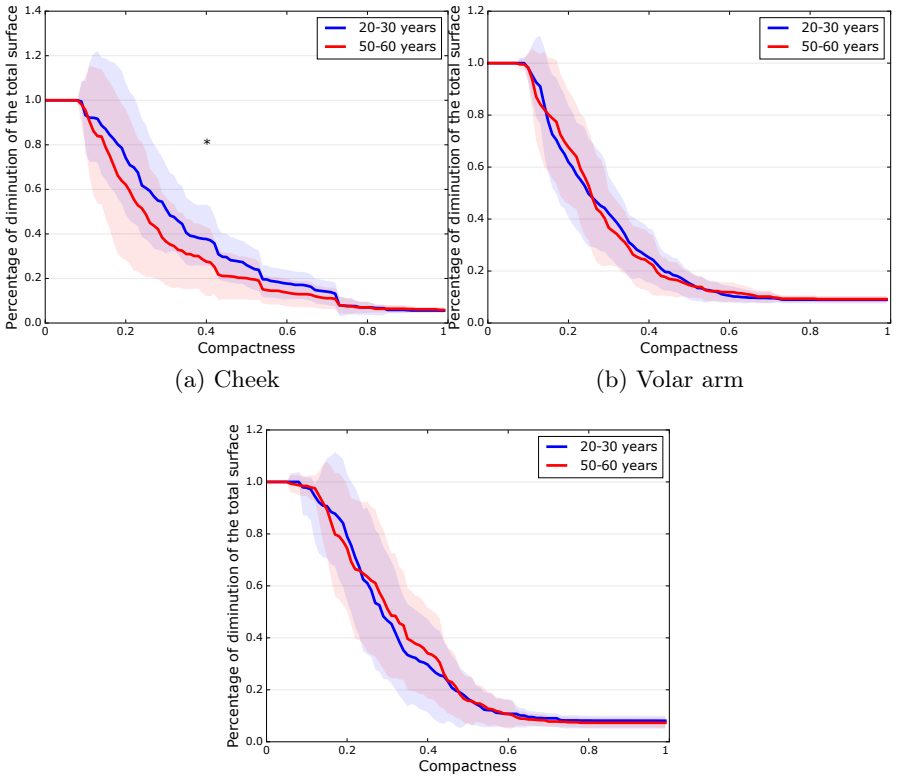

(a) Cheek (b) Volar arm

(c) Dorsal forearm

Fig. 7: Mean and standard deviation of the pattern spectra $\rho^{\text{sarea}}_{\text{comp}}$ of the two age groups on the three acquisition locations.

In order to reduce the inter-subject variability, we study the pattern spectra expressed as a percentage of decrease of the surface area attribute. The average pattern spectra $\rho^{\text{sarea}}_{\text{comp}}$ computed for each group at each location are presented in Figure 7. The lines represent the mean values and the shadowed areas the standard deviations for each population (20-30 years old and 55-65 years old). The

pattern spectra for the epidermal surface on the cheek are statistically different. We do not find statistical differences on the other areas.

Finally, to obtain an aggregated descriptor of the DEJ shape, we study the area under the curve (AUC), of the pattern spectra. We present box-and-whisker plots of the AUC measure of the pattern spectra for the three acquisition locations (cheek, volar arm and dorsal forearm) in Figure 8. Parametric data are analyzed using Student's unpaired t-test and non-parametric data are subjected to a Mann–Whitney test. One can observe that the AUC of the pattern spectra is higher in the younger group than in the older group on the cheek. When comparing the volar arm (photo-protected) and the dorsal forearm (photo-exposed), the photo-ageing effect is quantified among both populations with a significant decrease of the AUC. Therefore, the AUC of the pattern spectra of the DEJ with a compactness attribute and a surface area measure is able to assess the chronological ageing on the cheek and the photo-ageing for our two populations.

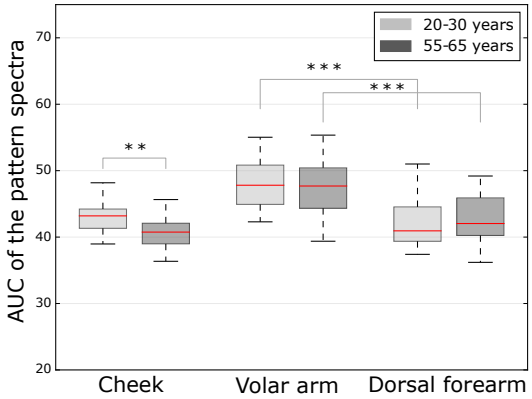

Fig. 8: Area under the curve of the pattern spectra. For each location and age group, we see: 1) the median AUC (central bar), 2) the first and third quartile (extremities of the box), and 3) the lowest datum still within 1.5 inter quartile range (difference between the third and first quartile) of the lower quartile, and the highest datum still within 1.5 inter quartile range of the upper quartile range (bottom and top extremities).

These results support our previous findings using local topological descriptors of the Tree-of-Shape regarding the chronological ageing on the DEJ on the cheek and photo-ageing among the young population [13]. However, the use of the pattern spectra brings more significant characteristics regarding the photo-aging among the older population compared to the local descriptors.

The proposed method also enriches the skin ageing descriptor focused on the automatic characterization of the epidermal cells in RCM images [14]. In future works, we plan to develop a novel method to automatically characterize the third significant ageing feature observable in skin RCM images: the dermal fibers.

References

1. Carlinet, E., Géraud, T.: Mtos: A tree of shapes for multivariate images. IEEE TIP **24**(12), 5330–5342 (2015)
2. Cavallaro, G., Mura, M.D., Benediktsson, J.A., Plaza, A.: Remote sensing image classification using attribute filters defined over the tree of shapes. IEEE GRS **54**(7), 3899–3911 (2016)
3. Dalla Mura, M., Benediktsson, J., Bruzzone, L.: Self-dual attribute profiles for the analysis of remote sensing images. In: ISMM. pp. 320–330 (2011)
4. Dalla Mura, M., Benediktsson, J., Waske, B., Bruzzone, L.: Morphological attribute profiles for the analysis of very high resolution images. IEEE GRS **48**(10), 3747–3762 (2010)
5. Géraud, T., Carlinet, E., Crozet, S., Najman, L.: A quasi-linear algorithm to compute the tree of shapes of nd images. In: ISMM. pp. 98–110 (2013)
6. Lavker, R.M., Zheng, P., Dong, G.: Aged skin: a study by light, transmission electron, and scanning electron microscopy. Journal of investigative dermatology **88** (1987)
7. Longo, C., Casari, A., Beretti, F., Cesinaro, A.M., Pellacani, G.: Skin aging: in vivo microscopic assessment of epidermal and dermal changes by means of confocal microscopy. Jour. of the American Academy of Dermatology **68**(3), e73–e82 (2013)
8. Longo, C., Casari, A., Pace, B., Simonazzi, S., Mazzaglia, G., Pellacani, G.: Proposal for an in vivo histopathologic scoring system for skin aging by means of confocal microscopy. Skin Research and Technology **19**(1) (2013)
9. Luo, B., Zhang, L.: Robust autodual morphological profiles for the classification of high-resolution satellite images. IEEE GRS **52**(2), 1451–1462 (2014)
10. Maragos, P.: Pattern spectrum and multiscale shape representation. IEEE PAMI **11**(7), 701–716 (1989)
11. Monasse, P., Guichard, F.: Fast computation of a contrast-invariant image representation. IEEE TIP **9**(5), 860–872 (2000)
12. Rittié, L., Fisher, G.J.: Natural and sun-induced aging of human skin. Cold spring harbor perspectives in medicine **5**(1), a015370 (2015)
13. Robic, J.: Automated quantification of the skin aging process using in-vivo confocal microscopy. Theses, Université Paris Est (Jun 2018), https://hal.archives-ouvertes.fr/tel-01884978
14. Robic, J., Nkengne, A., Perret, B., Couprie, M., Talbot, H.: Automated quantification of the epidermal aging process using in-vivo confocal microscopy. In: IEEE ISBI. pp. 1221–1224 (2016)
15. Robic, J., Perret, B., Nkengne, A., Couprie, M., Talbot, H.: Classification of the dermal-epidermal junction using in-vivo confocal microscopy. In: IEEE ISBI. pp. 252–255 (2017)
16. Salembier, P., Oliveras, A., Garrido, L.: Antiextensive connected operators for image and sequence processing. IEEE TIP **7**(4), 555–570 (1998)
17. Urbach, E., Roerdink, J., Wilkinson, M.: Connected shape-size pattern spectra for rotation and scale-invariant classification of gray-scale images. IEEE PAMI **29**(2), 272–285 (2007)
18. Xu, Y., Carlinet, E., Géraud, T., Najman, L.: Efficient computation of attributes and saliency maps on tree-based image representations. In: ISMM. pp. 693–704 (2015)